Magnetic plasmon in coupled nanosandwich structure

Liu Qiu,[1] Shuming Wang,[1,*] Hui Liu,[1] Tao Li,[1] Shining Zhu,[1] and Xiang Zhang[2]

[1]*National Laboratory of Solid State Microstructures and Department of Physics, Nanjing University, Nanjing 210093, China*
[2]*5130 Etcheverry Hall, Nanoscale Science and Engineering Center, University of California, Berkeley, California 94720-1740, USA*
**Corresponding author: shumingwang_1981@163.com*

Received November 29, 2010; revised May 8, 2011; accepted May 9, 2011; posted May 9, 2011 (Doc. ID 138759); published June 9, 2011

We investigate the magnetic resonant modes in the coupled nanosandwich (CSW) structure, which can be considered a metamolecule composed of two meta-atoms (nanosandwiches). The coupling between two nanosandwiches leads to two magnetic resonant modes, the split of the single magnetic resonant mode. Moreover, the coupling effect in a more complicated system that consists of two closely placed CSWs is studied, where four magnetic resonant modes with different phase relationships between meta-atoms are observed. It is shown that the interaction between CSWs leads to this secondary split of the magnetic resonant mode. We further consider a one-dimensional metacrystal formed by a chain of CSWs, and directly observe the magnetic plasmon (MP) bands through the Fourier transformation approach. Modifying both the thickness of the middle metal layer of CSWs and the spacing between CSWs, one can efficiently engineer the MP band, and even open a bandgap. Such a CSW chain can even work as a subwavelength waveguide, which may have potential applications in nano-optics and photonics.

OCIS codes: 160.3918, 240.6680.

1. INTRODUCTION

Nowadays, metamaterials have attracted considerable interest for their new physics and excellent functionality [1,2], which cannot be obtained from the natural materials [3–6]. A good example is high-frequency negative magnetic permeability, which can be obtained from the magnetic resonance in different artificial metal structures, such as split ring resonators (SRRs); high-frequency negative magnetic permeability is able to provide magnetic resonance from GHz to 100 THz with structures ranging in size from millimeters to nanometers [7–9]. However, the resonant frequency of SRR structure has a limit because of the kinetic energy of electrons [10]. To overcome such a limit, scientists have conceived of other new structures, such as the nanorod pair [11], fishnet structure [12–14], and nanosandwich structure [15,16] to increase the resonant frequency to even the visible region [17].

On the other hand, besides negative permeability, scientists have also paid attention to various phenomena that are due to the coupling effects in metamaterials [18,19]. A simple structure, such as an SRR or a metallic nanoparticle, can be considered a meta-atom, and a complicated system composed of several closely placed meta-atoms can be viewed as a metamolecule. In such a metamolecule, meta-atoms strongly couple with each other, and the hybridization effect will appear, leading to some interesting properties, such as hybridized energy levels [20] or plasmonic electromagnetic-induced transparency [21]. Moreover, coupled SRRs stacked with different directions can even provide chirality [22]. Once a large number of meta-atoms is regularly stacked, we can get a metacrystal, which has similar properties to those of the solid state crystal [23]. For example, the magnetic plasmon (MP) band can be obtained in a connected single SRR chain [24,25], and the optical-phononlike MP band is even observed in a diatomic slit-hole resonator chain [26]. A one-dimensional (1D) metacrystal composed of a chain of nanosandwiches has also been designed to get a higher frequency MP band [27].

In this paper, we investigate the magnetic resonant modes in the coupled nanosandwich (CSW) structure and the MP band in a 1D metacrystal composed of CSWs. The coupled system can provide additional properties that those simple systems cannot. The newly introduced hybridized magnetic resonant modes and magnetic plasmon bandgap may be useful in designing devices in nano-optics and photonics. The magnetic resonant modes resulting from the hybridization effect in a CSW are presented in Section 2. The complicated coupling properties in two closely stacked CSWs are also studied in Section 3. Furthermore, we investigate the MP band in a 1D CSW chain in Section 4. Finally, the conclusion is presented.

2. COUPLED NANOSANDWICH

As shown in the inset in Fig. 1, the CSW we studied can be considered a stack of two nanosandwiches with a shared metallic layer. According to the work of S. M. Wang *et al.* [27], the closed loop composed of free current and displacement current makes a magnetic resonator from a nanosandwich, which can be considered a meta-atom. In the CSW, two such meta-atoms couple with each other by current interaction in the shared metallic layer. We define the thickness of this metal layer as $\boldsymbol{d}$. Here, the metal component in the CSW is chosen to be silver with Drude type permittivity, $\varepsilon(\omega) = 1 - \omega_p^2/(\omega^2 + i\gamma\omega)$, where the bulk plasma frequency $\omega_p = 1.37 \times 10^{16}\,\mathrm{rad/s}$, and the relaxation rate $\gamma = 12.24 \times 10^{13}\,\mathrm{rad/s}$. The dielectric material is glass with an index of 1.5. The structural parameters of the CSW are $a = 300\,\mathrm{nm}$, $b = 350\,\mathrm{nm}$, $h = 50\,\mathrm{nm}$, and $\boldsymbol{d} = 25\,\mathrm{nm}$. In order to quantitatively study the magnetic resonance of a CSW, a commercial software package, CST MICROWAVE STUDIO (CST AG, Germany), is employed to obtain the numerical analysis.

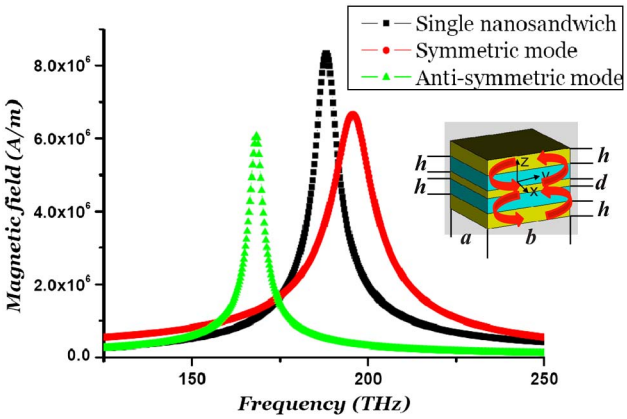

Fig. 1. (Color online) Magnetic field excited in a single nanosandwich and in a CSW. The geometry of a CSW is shown in the inset, where the yellow layers (top, middle, and bottom) correspond to the metallic layers and the blue layers (second and fourth) are dielectric layers.

We first provide the spectrum of excited magnetic resonance in a single nanosandwich labeled by the black dotted curve in Fig. 1. The parameters a and b are the same as given above, and the thicknesses of the three layers is $h/2$, h, and h, from top to bottom (exactly half of the CSW). It presents only one magnetic resonant frequency at 186 THz. A CSW can be considered a metamolecule composed of two meta-atoms (nanosandwiches). Because of the coupling between the two meta-atoms, the eigenmagnetic resonant mode splits into two resonant frequencies at $f_{01} = 196$ THz and $f_{02} = 168$ THz. To further investigate how the meta-atoms couple with each other, we present the distributions of the electric field, current density, and magnetic field at these two frequencies in the y–z plane in Fig. 2. The displacement current in the nonmetallic surrounding and the free current in the metallic slabs form two closed loops in the CSW, leading to two induced magnetic fields highly confined in the middle glass layers. According to the different phase relationships between the two excited magnetic fields, these two modes correspond to the symmetric mode at the high frequency and the antisymmetric mode at the low frequency, respectively. Figures 2(a)–2(c) present the field distributions of the symmetric mode, and Figs. 2(d)–2(f) correspond to the antisymmetric mode.

In the CSW, the thickness of the middle metallic layer, $\boldsymbol{d}$, directly determines the strength of the coupling, which plays a crucial part in the magnetic resonant frequency split from f_0 to f_{01} and f_{02}. We investigate the two eigenmodes in the CSW with $\boldsymbol{d}$ varying from 20 nm to 160 nm, shown in Fig. 3. Because of the strong coupling between the meta-atoms (nanosandwiches), the split of the two resonant frequencies is quite large with a small $\boldsymbol{d}$. As $\boldsymbol{d}$ increases, the coupling effect becomes weaker, and the split shrinks. When $\boldsymbol{d}$ is large enough, more than 100 nm, the split tends to zero, and the two modes degenerate to the same one.

In order to theoretically interpret this phenomenon, Lagrangian formalism is introduced to describe the coupling in the CSW [24]. In the CSW, each nanosandwich has an equivalent inductance–capacitance circuit with a capacitance C from the two silver slabs and a total inductance L, including the kinetic inductance, which is strongly dependent on the size of the nanostructure [10]. We define the charge accumulated in the system as a generalized coordinate, and the Lagrangian of a

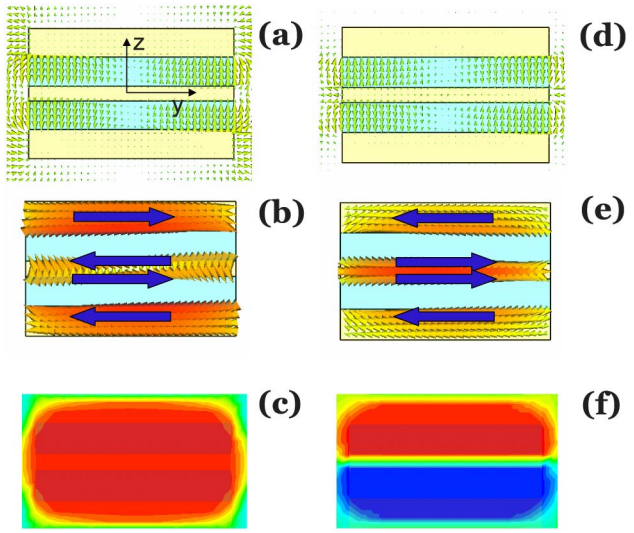

Fig. 2. (Color online) Electric field, free current, and magnetic field distribution in y–z plane ($x = 0$) of (a)–(c) the symmetric mode and (d)–(f) antisymmetric mode.

single nanosandwich can be expressed as $\Im = L\dot{q}^2/2 - q^2/2C$, where the two terms correspond to the energy stored in the inductor and the capacitor, respectively [24]. By solving the Euler–Lagrange equations, we can obtain the resonant frequency $\omega_0 = 1/\sqrt{LC}$, which is similar to the electromagnetic theory of LC circuits. In the CSW, we define q_1 and q_2 as the charges in each nanosandwich, and L and C as the induction and the capacitance of each nanosandwich. Then we can write the Lagrangian of the coupled system as

$$\Im = \frac{L}{2}(\dot{q}_1^2 + \dot{q}_2^2) - \frac{1}{2C}(q_1^2 + q_2^2) + \alpha\dot{q}_1\dot{q}_2, \tag{1}$$

where the first two terms respectively correspond to the energy stored in the inductors and capacitors. Here, considering the magnetic-inductive coupling between the two meta-atoms, the interaction term $\alpha\dot{q}_1\dot{q}_2$ is introduced. We introduce the magnetic momentum $\mu = A\dot{q}$, where A is the effective area of the magnetic loop of single meta-atom. By solving the Euler–Lagrange equations, we can obtain two eigenfrequencies

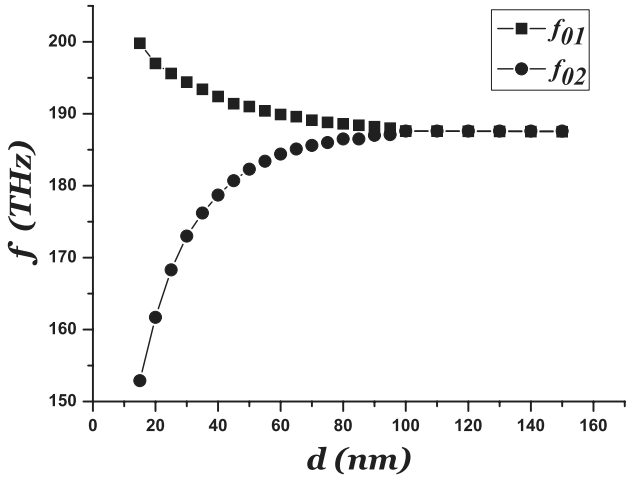

Fig. 3. Magnetic resonant frequencies of the symmetric mode and the antisymmetric mode.

$$f_{01}=\frac{\omega_1}{2\pi}=\frac{1}{2\pi}\sqrt{\frac{1}{L+\alpha}\frac{1}{C}} \quad \text{and} \quad f_{02}=\frac{\omega_2}{2\pi}=\frac{1}{2\pi}\sqrt{\frac{1}{L-\alpha}\frac{1}{C}}. \tag{2}$$

f_{01} is the symmetric mode with $\mu_1=\mu_2$, and f_{02} corresponds to the antisymmetric mode with $\mu_1=-\mu_2$. Here, α is negative, because of the different direction of the free current of q_1 and q_2 in the middle slab. This is consistent with the numerical results presented above and can be a theoretical proof of its validity. With the aid of the numerical simulation, magnetic coupled coefficient α can be calculated by using Eq. (2). For example, when $\boldsymbol{d}=50$ nm, we have $\alpha=0.14$. It should be mentioned that this method can only give a qualitative picture of the CSW, and the evaluation of the exact coupling strength is quite difficult.. Since the coupling is directly decided by $\boldsymbol{d}$, α is a function of $\boldsymbol{d}$. When $\boldsymbol{d}$ is small, $|\alpha|$ is large, which means that there is strong coupling between the two meta-atoms. As $\boldsymbol{d}$ increases, $|\alpha|$ decreases.

3. TWO COUPLED NANOSANDWICHES

After providing the magnetic resonant modes in a single CSW, we investigate the coupling effect in two closely placed CSWs, a more complicated metamolecule than a single CSW. The inset of Fig. 4 illustrates the way the two CSWs are placed. The parameters of the CSWs are the same as above. Here, the distance between the CSWs is chosen to be $\boldsymbol{p}=400$ nm. Figure 4 shows the spectrum of magnetic resonance excited in such a double CSW system. We can observe four eigenmagnetic resonant frequencies at $f_{11}=174.5$ THz, $f_{21}=166.2$ THz, $f_{31}=206.8$ THz, and $f_{41}=171.8$ THz. The distributions of the electric field, current density, and the magnetic field in the y–z plane are presented at these four frequencies in Figs. 5 and 6. In Fig. 5, the distributions of the magnetic field at f_{11} and f_{31} are plotted with the magnetic field inside the CSWs being symmetric. In Fig. 6, the distribution of the magnetic field in CSW is antisymmetric at f_{21} and f_{41}.

Different from the current interaction in the single CSW case, in this double CSWs system, another kind of coupling between the CSWs through the electromagnetic field overlap is introduced, which leads to a secondary magnetic resonant frequency split. In Fig. 4, the former antisymmetric mode f_{01} further splits into f_{11} and f_{31} ($f_{11}<f_{01}<f_{31}$) and another

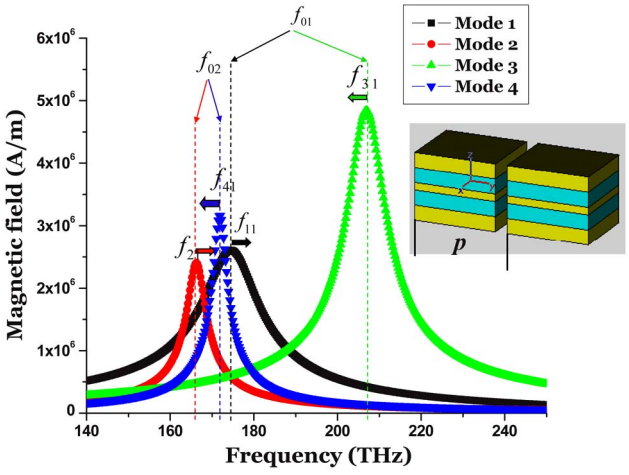

Fig. 4. (Color online) Magnetic field excited in two coupled CSW systems. The geometry of the system is shown in the inset.

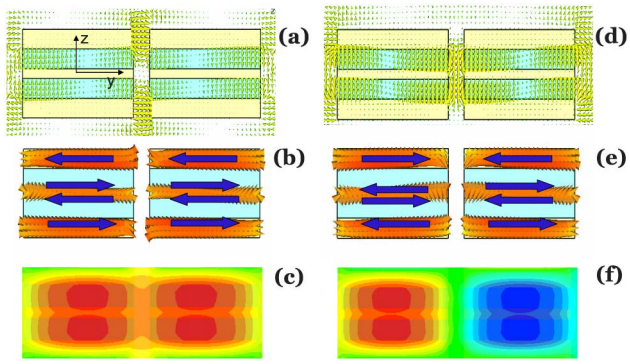

Fig. 5. (Color online) Electric field, free current, and magnetic field distribution in y–z plane ($x=0$) at (a)–(c) f_1 and (d)–(f) f_3.

secondary split exists around the former symmetric mode f_{02} ($f_{21}<f_{02}<f_{41}$). We have $\Delta_1 f=f_{31}-f_{11}=32.3$ THz, $\Delta_2 f=f_{41}-f_{21}=5.6$ THz. The strength of the new kind of coupling is strongly dependent on the spacing, $\boldsymbol{p}$, between the two CSWs. To figure out how $\boldsymbol{p}$ affects the system, we change $\boldsymbol{p}$ to 450 nm and keep the other parameters unchanged. Four new peaks at $f_{12}=185.8$ THz, $f_{22}=168.8$ THz, $f_{32}=203.8$ THz, and $f_{42}=170.5$ THz are obtained, where the second subscript "2" means the second case. The horizontal arrows show the movements of magnetic resonant frequencies in Fig. 4. The frequency splits still exist with $\Delta_1' f=f_{32}-f_{12}=18$ THz and $\Delta_2' f=f_{42}-f_{22}=1.7$ THz, while $\Delta_1 f>\Delta_1' f$ and $\Delta_2 f>\Delta_2' f$, which results from the decreasing of the coupling between theCSWs.

The Lagrangian formalism is also used to describe such double CSW systems. We define q_i and q_i' as the oscillation charges for a single CSW. For double CSWs, the coupling effect between the two CSWs is taken into consideration. Then we can also write the Lagrangian of the system,

$$\begin{aligned}\Im=&\frac{L}{2}(\dot{q}_1^2+\dot{q}_1'^2+\dot{q}_2^2+\dot{q}_2'^2)-\frac{1}{2C}(q_1^2+q_1'^2+q_2^2+q_2'^2)\\&+\alpha[\dot{q}_1\dot{q}_1'+\dot{q}_2\dot{q}_2']-\frac{1}{2C_1}[(q_1-q_2)^2+(q_1'-q_2')^2],\end{aligned} \tag{3}$$

where the first three terms correspond to the energy in two independent CSWs, and $\frac{1}{2C_1}[(q_1-q_2)^2+(q_1'-q_2')^2]$ is due to the electric field coupling effects between the two CSWs. Because the magnetic fields are highly confined in the glass layer along the x axis direction in a single CSW, the coupling effects of magnetic fields between the adjacent CSWs can be neglected compared with the strong electric field coupling

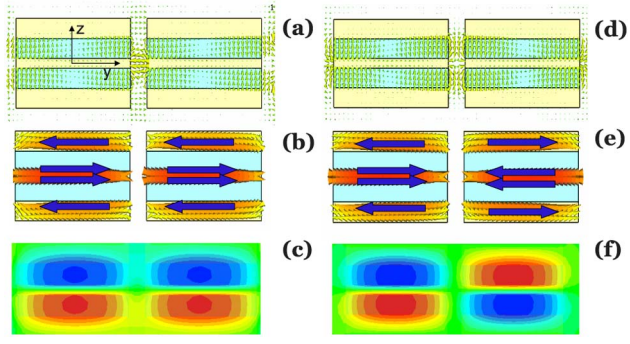

Fig. 6. (Color online) Electric field, free current, and magnetic field distribution in y–z plane ($x=0$) at (a)–(c) f_2 and (d)–(f) f_4.

effects for the small spacing between CSWs. This differs from the case in the connected SRRs system [24,25], in which the strong current interaction, the term related to $\dot{q}$, plays a major role. After solving the Euler–Lagrange equations, four resonant frequencies can be obtained at

$$f_1 = \frac{1}{2\pi}\sqrt{\frac{1}{L+\alpha}\frac{1}{C}}, \qquad f_2 = \frac{1}{2\pi}\sqrt{\frac{1}{L-\alpha}\frac{1}{C}},$$
$$f_3 = \frac{1}{2\pi}\sqrt{\frac{1}{L+\alpha}\left(\frac{1}{C}+\frac{2}{C_1}\right)}, \qquad f_4 = \frac{1}{2\pi}\sqrt{\frac{1}{L-\alpha}\left(\frac{1}{C}+\frac{2}{C_1}\right)}. \tag{4}$$

Here, $f_3 > f_1$ and $f_4 > f_2$. We have $\mu_1 = \mu_1' = \mu_2 = \mu_2'$ at f_1; $\mu_1 = -\mu_1' = \mu_2 = -\mu_2'$ at f_2; $\mu_1 = \mu_1' = -\mu_2 = -\mu_2'$ at f_3; and $\mu_1 = -\mu_1' = -\mu_2 = \mu_2'$ at f_4. The symmetry of these different modes is the same as the result obtained from the distribution of the magnetic field in Figs. 5 and 6. As $\boldsymbol{p}$ increases, the parameter C_1, which decides the strength of coupling effect, decreases and both frequency splits $\Delta_1 f = \frac{1}{2\pi}\sqrt{\frac{1}{L-\alpha}}\left(\sqrt{\frac{1}{C}+\frac{1}{C_1}} - \sqrt{\frac{1}{C}}\right)$ and $\Delta_2 f = \frac{1}{2\pi}\sqrt{\frac{1}{L+\alpha}}\left(\sqrt{\frac{1}{C}+\frac{1}{C_1}} - \sqrt{\frac{1}{C}}\right)$ decline.

4. COUPLED NANOSANDWICH CHAIN

When we use the meta-atoms to form a metacrystal, for example a 1D system, we can get the collective magnetic resonant mode (magnetic plasmon) in the system, which is quite similar to the collective vibration in the crystal lattice [27–30]. And if the meta-atom is replaced with a complex metamolecule with two eigenmodes, such as a CSW, the result will be quite interesting and of rich physics.

Our 1D structure is composed of a chain of 20 CSWs, which is about 8 μm and far beyond the wavelength at the frequency of more than 100 THz. As a result, we could no longer use the quasi-static approximation used above, and we need to take the retardation and the high-order interactions into consideration [31–33], which is quite difficult for theoretical derivation. Therefore, the numerical simulation is a good choice for investigation on such a chain. Figure 7(a) shows a 1D CSW chain and the exciting current source. In this system, a, b, h, $\boldsymbol{d}$, and $\boldsymbol{p}$ are 200 nm, 300 nm, 50 nm, 25 nm, and 400 nm, respectively. The magnetic field distributions at different frequencies $H(\omega, y)$ can be obtained through numerical simulation. A Fourier transformation (FT) method, $H(\omega, k) = \int H(\omega, y)\, e^{iky} \mathrm{d}y$, is employed to get the magnetic field information in the wave vector region, so that we can easily observe the magnetic plasmon modes excited in the chain according to their value [27,30]. An FT map is shown in Fig. 7(b), with the brightness indicating the strength of $H(\omega, k)$. There exist two magnetic plasmon bands marked by a red rectangular box (inner box) and a yellow rectangular box (outer box). The former corresponds to the antisymmetric MP mode with a bandwidth of about 20 THz, ranging from 158 THz to 178 THz. The latter band is the symmetric MP mode with a width of about 92 THz, ranging from 129 THz to 221 THz. These two bands have an overlap at about 165 THz, and the magnetic field here is much stronger because of the coexistence of both symmetric and antisymmetric MP modes. In addition, it is found that the modes in the symmetric MP band are stronger than those of the antisymmetric band, because the symmetric modes are much easier to excite by the current source than the antisymmetric modes.

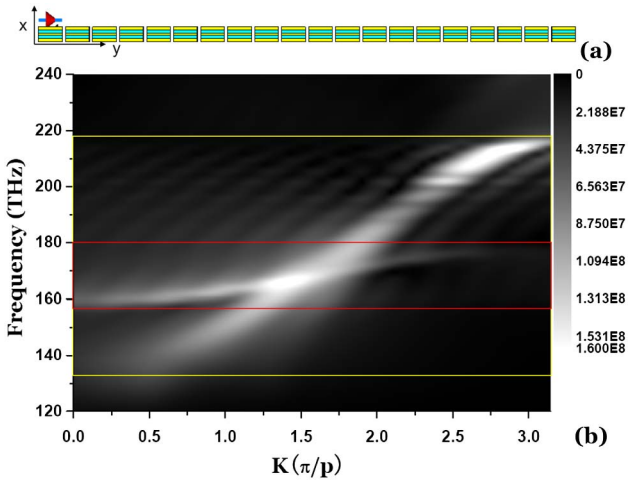

Fig. 7. (Color online) (a) Structure of the CSW chain, (b) Dispersion relationship of the CSW chain with $a = 200$ nm, $b = 300$ nm, $\boldsymbol{p} = 400$ nm, and $\boldsymbol{d} = 25$ nm.

The physics mechanism of the 1D CSW system can be divided into two parts of the coupling effect. First, the coupling between two meta-atoms in the CSW results in the first split of eigenmagnetic resonant frequency, $f_0 \rightarrow f_{01}, f_{02}$. As shown in Fig. 8, when two CSWs are placed side by side, the interaction between the adjacent CSWs leads to the secondary frequency splits, $f_{01} \rightarrow f_3, f_1$ while $f_{02} \rightarrow f_4, f_2$. When a large number of CSWs are coupled with each other, two magnetic plasmon bands will form, corresponding to the gray blocks in Fig. 8. The location of the band is directly determined by f_{01} and f_{02}. In addition, the bandwidth of these two bands strongly depends on the interaction between the CSWs. Therefore, we can modulate the 1D CSW system in two ways, by changing $\boldsymbol{d}$ and $\boldsymbol{p}$. The former directly determines the property of a single CSW and the latter presents the information about the chain.

We first compare cases with $\boldsymbol{d} = 25$ nm and 40 nm, while keeping $\boldsymbol{p} = 400$ nm unchanged. The FT maps of both cases are presented in Figs. 9(a) and 9(b), respectively. In Fig. 9(a), we obtain a symmetric MP mode with a width of about 65 THz, ranging from 155 THz to 220 THz. We get an antisymmetric MP mode with a width of about 15 THz, ranging from 161 THz to 176 THz. In Fig. 9(b), although with different $\boldsymbol{d}$, we obtain a similar bandwidth of symmetric MP mode as the former case, at about 62 THz, ranging from 156 THz to 218 THz, which may be due to the unchanged coupling between the CSWs. We also observe an antisymmetric MP mode with a width of about 16 THz, ranging from 173 THz to 189 THz, which owns a

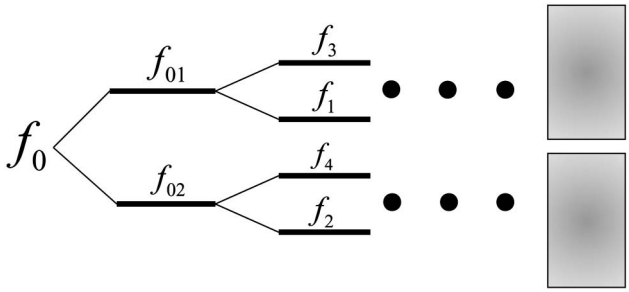

Fig. 8. Energy band diagram of CSW chain.

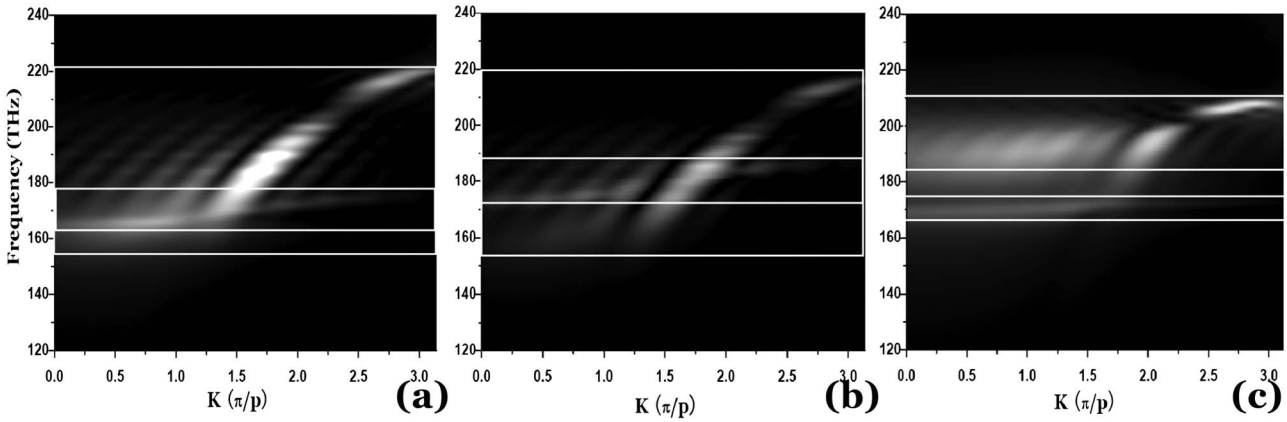

Fig. 9. (a) Dispersion relationship of the CSW chain with $a = 200$ nm, $b = 300$ nm, $\boldsymbol{p} = 400$ nm, and $\boldsymbol{d} = 25$ nm; (b) dispersion relationship of the CSW chain with $a = 200$ nm, $b = 300$ nm, $\boldsymbol{p} = 400$ nm, and $\boldsymbol{d} = 40$ nm; (c) dispersion relationship of the CSW chain with $a = 200$ nm, $b = 300$ nm, $\boldsymbol{p} = 500$ nm, and $\boldsymbol{d} = 25$ nm.

similar bandwidth as the former case. However, the center frequency, which determines the location of the MP band, of the two cases is different, especially in the antisymmetric case. This means that one can efficiently tune the MP band location of the CSW chain by changing the height of the middle metal slab of the CSW, $\boldsymbol{d}$. The other way to tune the MP band is to change the period, $\boldsymbol{p}$, of the chain. We change $\boldsymbol{p} = 500$ nm while $\boldsymbol{d} = 25$ nm remains unchanged. This time, we observe a symmetric MP mode with a width of about 26 THz, ranging from 182 THz to 208 THz and an antisymmetric MP mode with a width of about 8 THz, ranging from 168 THz to 176 THz. It can be concluded that the bandwidths of both the symmetry band and the antisymmetric band can be efficiently modified by tuning the period $\boldsymbol{p}$. In addition, in Fig. 9(c), we can even get a bandgap when we increase the period and reduce the interaction between the CSWs. In the metacrystal composed of CSWs, we get one more freedom degree, $\boldsymbol{d}$, to modify the coupling inside the the CSW, which leads to an additional MP band. Together with changing the period $\boldsymbol{p}$, we can implement a variety of MP band engineering techniques and get both bands and gaps from the dispersion relationship that the nanosandwich system cannot provide [27].

It should also be mentioned that such a CSW chain can be used as an MP waveguide. The strong modes at the high-frequency part are well able to propagate a field for the large wave vector that cannot leak to free space. Moreover, because of the high confinement of the electromagnetic field in the CSW, such a waveguide is a subwavelength waveguide. The power flow in it is strongly localized to the waveguide itself, which leads to the subwavelength property. In the MP band (about 213 THz), the power flow at the cross section with $y = 3500$ nm is shown in Fig. 10(a). The power flow at $z = 0$ along the chain is also plotted. The power flow does not decrease fast along the chain, except at the input part, where a peak results directly from the exciting source.

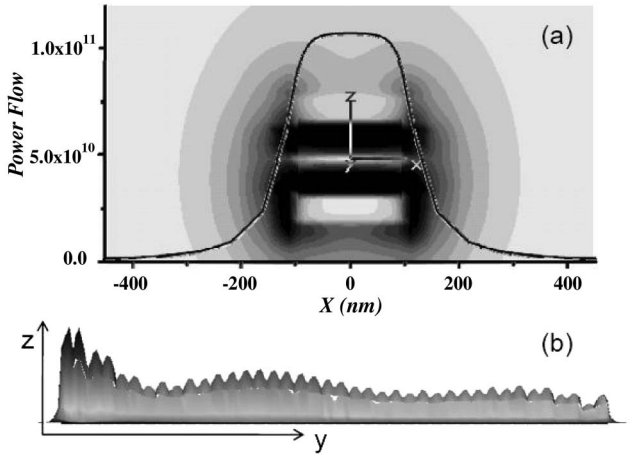

Fig. 10. (a) Power flow at cross section with $y = 3500$ nm; (b) power flow at $z = 0$ along the chain.

5. CONCLUSION

In summary, we first investigate the two eigenmagnetic resonant modes in the CSW, which can be considered the eigenfrequency split in a diatomic metamolecule composed of two meta-atoms. Then, a more complicated system that consists of two closely placed CSWs is studied, in which four eigenmodes are observed. The spacing between CSWs directly decides the strength of the interaction between the CSWs that leads to the secondary split of the eigenmagnetic resonant mode. We further consider a 1D metacrystal formed by a chain of CSWs and observe the MP bands through the FT map. Modifying both the thickness of the middle metal layer, $\boldsymbol{d}$, of the CSWs and the spacing between CSWs, $\boldsymbol{p}$, can efficiently engineer the MP band and even open a bandgap. Such a CSW chain can even work as a subwavelength waveguide, which may have potential applications in nano-optics and photonics.

ACKNOWLEDGMENTS

This work is supported by the National Programs of China (grants 51001059, 11074119, 11011120243, 10904012, and 10874081).

REFERENCES

1. E. Shamonina, V. A. Kalinin, K. H. Ringhofer, and L. Solymar, "Magnetoinductive waves in one, two, and three dimensions," J. Appl. Phys. **92**, 6252–6261 (2002).
2. M. Beruete, F. Falcone, M. J. Freire, R. Marqués, and J. D. Baena, "Electroinductive waves in chains of complementary metamaterial elements," Appl. Phys. Lett. **88**, 083503 (2006).
3. J. B. Pendry, "Negative refraction makes a perfect lens," Phys. Rev. Lett. **85**, 3966–3969 (2000).
4. N. Fang, H. Lee, C. Sun, and X. Zhang, "Sub—diffraction-limited optical imaging with a silver superlens," Science **308**, 534–537 (2005).

5. J. B. Pendry, D. Schurig, and D. R. Smith, "Controlling electromagnetic fields," Science **312**, 1780–1782 (2006).
6. R. Liu, C. Ji, J. J. Mock, J. Y. Chin, T. J. Cui, and D. R. Smith, "Broadband ground-plane cloak," Science **323**, 366–369 (2009).
7. R. A. Shelby, D. R. Smith, and S. Schultz, "Experimental verification of a negative index of refraction," Science **292**, 77–79 (2001).
8. T. J. Yen, W. J. Padilla, N. Fang, D. C. Vier, D. R. Smith, J. B. Pendry, D. N. Basov, and X. Zhang, "Terahertz magnetic response from artificial materials," Science **303**, 1494–1496 (2004).
9. S. Linden, C. Enkrich, M. Wegener, J. Zhou, T. Koschny, and C. M. Soukoulis, "Magnetic response of metamaterials at 100 terahertz," Science **306**, 1351–1353 (2004).
10. J. Zhou, T. Koschny, M. Kafesaki, E. N. Economou, J. B. Pendry, and C. M. Soukoulis, "Saturation of the magnetic response of split-ring resonators at optical frequencies," Phys. Rev. Lett. **95**, 223902-1–223902-4 (2005).
11. V. M. Shalaev, W. Cai, U. K. Chettiar, H. Yuan, A. K. Sarychev, V. P. Drachev, and A. V. Kildishev, "Negative index of refraction in optical metamaterials," Opt. Lett. **30**, 3356–3358 (2005).
12. S. Zhang, W. Fan, N. C. Panoiu, K. J. Malloy, R. M. Osgood, and S. R. J. Brueck, "Experimental demonstration of near-infrared negative-index metamaterials," Phys. Rev. Lett. **95**, 137404-1–137404-4 (2005).
13. G. Dolling, C. Enkrich, M. Wegener, C. M. Soukoulis, and S. Linden, "Simultaneous negative phase and group velocity of light in a metamaterial," Science **312**, 892–894 (2006).
14. T. Li, H. Liu, F. M. Wang, Z. G. Dong, S. N. Zhu, and X. Zhang, "Coupling effect of magnetic polariton in perforated metal/dielectric layered metamaterials and its influence on negative refraction transmission," Opt. Express **14**, 11155–11163 (2006).
15. L. V. Panina, A. N. Grigorenko, and D. P. Makhnovskiy, "Optomagnetic composite medium with conducting nanoelements," Phys. Rev. B **66**, 155411 (2002).
16. S. Zhang, W. Fan, K. J. Malloy, S. R. Brueck, N. C. Panoiu, and R. M. Osgood, "Near-infrared double negative metamaterials," Opt. Express **13**, 4922–4930 (2005).
17. H. K. Yuan, U. K. Chettiar, W. Cai, A. V. Kildishev, A. Boltasseva, V. P. Drachev, and V. M. Shalaev, "Negative permeability material at red light," Opt. Express **15**, 1076–1083 (2007).
18. H. Liu, Y. M. Liu, T. Li, S. M. Wang, S. N. Zhu, and X. Zhang, "Coupled magnetic plasmons in metamaterials," Phys. Status Solidi B **246**, 1397–1406 (2009).
19. H. Liu, Y. M. Liu, T. Li, S. M. Wang, S. N. Zhu, and X. Zhang, Chapter 11 in *Metamaterials Theory, Design and Applications*, T. J. Cui, D. R. Smith, and R. P. Liu, eds. (Springer, 2009), pp. 247–269.
20. N. Liu, H. Liu, S. N. Zhu, and H. Giessen, "Stereometamaterials," Nat. Photon. **3**, 157–162 (2009).
21. S. Zhang, D. A. Genov, Y. Wang, M. Liu, and X. Zhang, "Plasmon-induced transparency in metamaterials," Phys. Rev. Lett. **101**, 047401-1–047401-4 (2008).
22. H. Liu, D. A. Genov, D. M. Wu, Y. M. Liu, Z. W. Liu, C. Sun, S. N. Zhu, and X. Zhang, "Magnetic plasmon hybridization and optical activity at optical frequencies in metallic nanostructures," Phys. Rev. B **76**, 073101 (2007).
23. O. Sydoruk, O. Zhuromskyy, E. Shamonina, and L. Solymar, "Phonon-like dispersion curves of magnetoinductive waves," Appl. Phys. Lett. **87**, 072501 (2005).
24. H. Liu, D. A. Genov, D. M. Wu, Y. M. Liu, J. M. Steele, C. Sun, S. N. Zhu, and X. Zhang, "Magnetic plasmon propagation along a chain of connected subwavelength resonators at infrared frequencies," Phys. Rev. Lett. **97**, 243902-1–243902-4 (2006).
25. T. Li, R. X. Ye, C. Li, H. Liu, S. M. Wang, J. X. Cao, S. N. Zhu, and X. Zhang, "Structural-configurated magnetic plasmon bands in connected ring chains," Opt. Express **17**, 11486–11494 (2009).
26. H. Liu, T. Li, Q. J. Wang, Z. H. Zhu, S. M. Wang, J. Q. Li, S. N. Zhu, Y. Y. Zhu, and X. Zhang, "Extraordinary optical transmission induced by excitation of a magnetic plasmon propagation mode in a diatomic chain of slit-hole resonators," Phys. Rev. B **79**, 024304 (2009).
27. S. M. Wang, T. Li, H. Liu, F. M. Wang, S. N. Zhu, and X. Zhang, "Magnetic plasmon modes in periodic chains of nanosandwiches," Opt. Express **16**, 3560–3565 (2008).
28. G. Dolling, M. Wegener, A. Schädle, S. Burger, and S. Linden, "Observation of magnetization waves in negative-index photonic metamaterials," Appl. Phys. Lett. **89**, 231118 (2006).
29. N. Liu, S. Kaiser, and H. Giessen, "Magnetoinductive and electroinductive coupling in plasmonic metamaterial molecules," Adv. Mater. **20**, 4521–4525 (2008).
30. S. M. Wang, T. Li, H. Liu, F. M. Wang, S. N. Zhu, and X. Zhang, "Selective switch made from a graded nanosandwich chain," Appl. Phys. Lett. **93**, 233102 (2008).
31. W. H. Weber and G. W. Ford, "Propagation of optical excitations by dipolar interactions in metal nanoparticle chains," Phys. Rev. B **70**, 125429 (2004).
32. V. Lomanets, O. Zhuromskyy, G. Onishchukov, O. Sydoruk, E. Tatartschuk, E. Shamonina, G. Leuchs, and U. Peschel, "Interacting waves on chains of split-ring resonators in the presence of retardation," J. Appl. Phys. **106**, 104908 (2009).
33. M. Decker1, S. Burger, S. Linden, and M. Wegener, "Magnetization waves in split-ring-resonator arrays: evidence for retardation effects," Phys. Rev. B **80**, 193102 (2009).